HiSST: 3rd International Conference on
High-Speed Vehicle Science & Technology
14–19 April 2024, Busan, Korea

# Ablation measurements on aluminium spheres in a hyperballistic tunnel

*Flavien DENIS*[*1], *Hermann ALBERS*[*2], *Myriam BASTIDE*[*3], *Christian REY*[*4],
Serge GAISSER[*5], Daniel ROTHER[*6], Thierry STEIBLIN[*7]

## Abstract

The aim of this study is to experimentally measure the ablation of aluminium spheres in hypersonic free flight. The experiment is carried out in the ISL hyperballistic tunnel. The $8$ mm aluminium spheres are accelerated up to $4000\,\mathrm{m \cdot s^{-1}}$ and performed a decelerated free flight in a tunnel of $21$ m. Several measurements, such as velocity measurements, flash radiography and high speed imaging are performed during the free flight to detect and to measure the ablation. In addition, some models are recovered for post-flight analysis. The ablation profiles are extracted using an image post-processing algorithm. The results highlight the contribution of the oxidation to the ablation phenomenon and provide experimental results for the validation of the numerical tools.

**Keywords:** *ablation, metallic materials, free flight experiment, hyperballistic tunnel, hypersonic flow*

## Nomenclature

*Latin*

$A$ – Coefficient [$\mathrm{m^{-1}}$]
$a$ – Thermal diffusivity [$\mathrm{m^2 \cdot s^{-1}}$]
– or Acceleration [$\mathrm{m \cdot s^{-2}}$ or $\mathrm{m \cdot s^{-1} \cdot m^{-1}}$]
$B$ – Coefficient [$\mathrm{s \cdot m^{-1}}$]
$C$ – Coefficient [m]
$Cp$ – Heat capacity [$\mathrm{J \cdot kg^{-1} \cdot K^{-1}}$]
$C_L$ – Deceleration coefficient [-]
$C_x$ – Drag coefficient [-]
$D$ – Projectile reference diameter [mm]
$E$ – Thermal effusivity [$\mathrm{W \cdot s^{0.5} \cdot m^{-2} \cdot K^{-1}}$]
$m$ – Projectile mass [kg]
$p$ – Pressure [Pa]
$T$ – Temperature [K]
$t$ – Time [s]
$v$ – Velocity [$\mathrm{m \cdot s^{-1}}$]
$X$ – Position [m]
$x$ – Position [m]
– or Horizontal position [mm]
$y$ – Vertical position [mm]

*Greek*

$\Delta_{exp}$ – Exposure time [ns]
$\Delta H_f$ – Latent heat of fusion [$\mathrm{J \cdot kg^{-1}}$]
$\lambda$ – Thermal heat conductivity [$\mathrm{W \cdot m^{-1} \cdot K^{-1}}$]
$\rho$ – Density [$\mathrm{kg \cdot m^{-3}}$]

*Subscripts*

$f$ – Fusion
$tank$ – Expansion tank
$tunnel$ – Measurement tunnel
$v$ – Vaporisation
$0$ – Initial condition

*Acronyms*

ISL – French-German Research Institute of Saint-Louis

[1]*Research Scientist, Aerodynamics, Measurements & Simulations, flavien.denis@isl.eu*
[2]*Research engineer, Aerodynamics, Measurements & Simulations, hermann.albers@isl.eu*
[3]*Research engineer, Aerodynamics, Measurements & Simulations, myriam.bastide@isl.eu*
[4]*Research engineer, Aerodynamics, Measurements & Simulations, christian.rey@isl.eu*
[5]*Pyrotechnician, Aerodynamics, Measurements & Simulations, serge.gaisser@isl.eu*
[6]*Pyrotechnician, Aerodynamics, Measurements & Simulations, daniel.rother@isl.eu*
[7]*Pyrotechnician, Aerodynamics & Exterior Ballistics, thierry.steiblin@isl.eu*
[*]French-German Research Institute of Saint-Louis, 5 rue du Général Cassagnou - BP 70034, 68301 Saint-Louis Cedex - France

## 1. Introduction

Thermal ablation in hypersonic flight has been studied for many years as a research topic dedicated to the design of thermal protection systems for re-entry vehicles. Recently, new ablation challenges have emerged, such as the destruction of end-of-life satellites during atmospheric re-entry, or the protection of future hypersonic projectiles against ablation. Both applications involve the ablation of non-thermally protected metallic materials.

Ablation, the process by which material is removed from the surface of an object due to the aerothermal heating during an hypersonic flight, plays a fundamental role in both the re-entry of space debris and the performance of hypersonic projectiles. Metallic materials, known for their strength, durability, and thermal properties, are commonly used in the construction of spacecraft components, and hypersonic vehicles. However, the behaviour of these materials under the high thermal loads encountered during re-entry and hypersonic flight remains a subject of active investigation.

The experimental study of the ablation phenomenon is complicated by the fact that the experimental facility must be able to generate a high enthalpy flow for a period of time long enough to induce a degradation of the material. Plasma torches are commonly used because of their ability to reproduce realistic aerothermal conditions at the surface of the models. However, reproducing realistic flow conditions at positions other than the stagnation point is difficult. A second approach is to use substitutive ablative materials, such as Teflon, naphthalene or gallium, to study ablation over short period of time in shock wind tunnels or low enthalpy wind tunnels but the substitutive material does not behave exactly like the material used in flight.

This article describes an other experimental method developed for the ablation study of metallic materials in hypersonic free flight. The ISL hyperbalistic tunnel is used to study the ablation aluminium spheres in a dense atmosphere.

## 2. Experimental setup

### 2.1. ISL hyperballistic tunnel

The ISL hyperballistic tunnel belongs to the category of hypersonic ballistic ranges. It is used to study hypersonic free flight and hypervelocity impacts. The facility consists of two parts: a hypersonic launcher and a free flight tunnel. A schematic of the facility is shown in Fig. 1a.

The model is accelerated by a two-stage light gas gun, as shown in Fig. 1b. The first stage is a powder chamber and the second stage is a high pressure chamber. The two stages are filled with hydrogen and are separated by a piston. The combustion of the powder in the first stage forces the piston to move in the high-pressure chamber, thus compressing the hydrogen. At a pre-defined pressure, a membrane located at the end of the high-pressure chamber breaks and the hydrogen at high pressure expands into the launch tube, thereby accelerating the projectile to hypersonic speeds ranging from $2000\,\mathrm{m \cdot s^{-1}}$ to $9000\,\mathrm{m \cdot s^{-1}}$. The launch tube of calibre $11.7\,\mathrm{mm}$ is selected for the present study.

From the muzzle of the gun, the projectile enters the free flight tunnel, which is presented in Fig. 1c. The transitional ballistic phase takes place in an expansion tank, where the muzzle blast is damped and the sabots, which guide the projectile into the launch tube, open and release the model. Then, the projectile enters the measurement tunnel. This tunnel is equipped with optical accesses for visualisations and measurements during free flight. At the end of the tunnel, a soft recovery system based on plastic foam allows the projectile to be recovered for post-flight analysis. The total length of the free flight phase is $21\,\mathrm{m}$. The tunnel is also completely isolated from the laboratory atmosphere, so that the mixture and pressure of the test gas can be modified to suit experimental requirements.

### 2.2. Models

The projectile tested is a duralumin sphere with a diameter of $8\,\mathrm{mm}$ and a mass of $0.71 \pm 0.02\,\mathrm{g}$. 24 models are tested. The aluminium is chosen for its low melting point of $850\,\mathrm{K}$, so that the ablation can be initiated during the free flight in the hyperballistic tunnel. With a calibre of $8\,\mathrm{mm}$, the inertia is low enough to decelerate the projectile before it enters the soft recovery system. So, it can be recovered with a minimum of damage. The drawback is that the velocity of the projectile is not constant during


**(a)** Overview of the facility

**(b)** Two-stage light gas gun

**(c)** Measurement tunnel

**Fig 1.** ISL hyperballistic tunnel

the flight. The thermophysical properties of the duralumin spheres are summarised in Table 1.

**Table 1.** Thermophysical properties at $293$ K. 1) From [1]. 2) From [2] 3) From [3]. 4) Data based on aluminium.

| | $\rho$ | $Cp$ | $\lambda$ | $a$ | $E$ | $T_f$ | $\Delta H_f$ |
|---|---|---|---|---|---|---|---|
| Duralumin | 2787[1] | 883[1] | 164[1] | 6.676E-5[1] | 2.01E+5[1] | 775-910[2] | 3.56E+5[3&4] |

During the acceleration inside the gun, the sphere is packed in a polycarbonate packet made of four sabots and a pusher plate. At the gun muzzle, it opens because of the aerodynamic forces and releases the projectile. A picture of the projectile with its sabots is shown in Fig. 2.

## 2.3. Measurement setup

### *2.3.1. Velocity measurements*

The measurement tunnel is equipped with four speed measurement stations. Each station consists of a pair of light barriers. On one side of the tunnel, a laser sheet is generated by a polarised helium-neon laser and lenses. On the other side, a lens focuses the laser sheet on a photodiode, which converts the light signal into an electrical one. A pass-band filter and a polarisation filter are also mounted on the detector. The projectile is detected when the variation of the electrical signal rises above a trigger value.

The times of each detection are used to calculate the 1D-trajectory of the projectile. The trajectory computation is based on a curve fitting. First an approximation of the coefficients $A$ and $B$ is estimated by using Equ. 1. Then the final estimation of the coefficients $A$, $B$ and $C$ is performed based on the Eqn. 2. From the value of the coefficient $A$, the drag coefficient of the sphere in free flight can be determined using Eqn. 3.

$$v(t) = \frac{1}{At + B} \tag{1}$$

**Fig 2.** 8mm-sphere with its sabots

$$x(t) = \frac{1}{A} \ln |At + B| + C \tag{2}$$

With:

$$A = \frac{1}{8} \frac{\rho \pi D^2 C_x}{m} \tag{3}$$

In addition to the calculation of the projectile speed, the light barrier signals are also used to trigger the other measuring devices.

#### *2.3.2. High speed imaging*

Several optical visualisations are performed throughout the measurement tunnel. At the gun muzzle, a Photron SAZ camera records the sabot opening sequence at $30\,000$ fps with an exposure time of $160$ ns. During the free flight phase, the visualisation of the sphere is achieved with three other high speed cameras and their respective illumination systems: a Specialized Imaging SIMD16 camera at $66\,225$ fps with an exposure time of $50$ ns illuminated by a Hensel $6000$ J flash, a Shimadzu HPV-X camera at $200\,000$ fps with an exposure time of $200$ ns illuminated by a Hensel $3000$ J flash and a Photron SAZ colour camera at $60\,000$ fps with an exposure time of $160$ ns illuminated by two LED lamps and a Dedolight projector. Finally, two PCO Sensicam cameras and their flash lamp are used to produce two single blur-free images thanks to their exposure time of $100$ ns.

#### *2.3.3. Flash radiography*

At hypersonic speeds, the strong bow shock and the light emission make it impossible to accurately visualise the stagnation region of the projectile. For this reason, three flash radiographies are performed during the free flight in order to obtain accurate visualisations of the projectile surface without being disturbed by the aforementioned phenomena. A flash radiography system is composed of a x-ray generator and a recording plate. The duration of the x-ray flash is approximately $25$ ns.

### 2.4. Test matrix

24 experiments are carried out within the hyperballistic tunnel. The test matrix is shown in Tab. 2. The tests are performed with two different test gas, pure nitrogen or dry air, to assess the effect of oxygen on ablation. Different test gas pressures are used in the measurement tunnel, ranging from $0.5$ bar to $2.0$ bar. For technical reasons, the pressure in the expansion tank is kept below $1$ bar. As the projectile approaches the end of the expansion tank, a quick-opening membrane opens, allowing the projectile to pass from the expansion tank into the measurement tunnel. Finally, the initial velocity is varied, ranging from $2900\,\mathrm{m \cdot s^{-1}}$ to $4020\,\mathrm{m \cdot s^{-1}}$.

**Table 2.** Test matrix

| Test number | Test gas | $p_{tank}$ | $p_{tunnel}$ | $v_{0,tunnel}$ $\pm 90 m \cdot s^{-1}$ | Projectile recovered |
|---|---|---|---|---|---|
| 1 | N2 | 0.5 | 0.5 | - | x |
| 2 | N2 | 0.9 | 0.9 | 3500 | x |
| 3 | N2 | 0.8 | 0.8 | 2900 | x |
| 4 | N2 | 0.3 | 1.5 | 3840 | x |
| 5 | N2 | 0.8 | 0.8 | 2780 | x |
| 6 | N2 | 0.4 | 1.2 | 3670 | x |
| 7 | N2 | 0.5 | 1.4 | 3390 | x |
| 8 | N2 | 0.5 | 1.6 | 3430 | x |
| 9 | N2 | 0.5 | 1.7 | 3450 | |
| 10 | N2 | 0.5 | 1.9 | 3880 | x |
| 11 | N2 | 0.5 | 1.3 | 3260 | x |
| 12 | Air | 0.5 | 2.0 | 3850 | x |
| 13 | Air | 0.5 | 2.0 | 4230 | |
| 14 | N2 | 0.5 | 1.8 | 3450 | x |
| 15 | N2 | 0.5 | 1.7 | 3540 | x |
| 16 | N2 | 0.5 | 2.0 | 3470 | x |
| 17 | N2 | 0.5 | 2.0 | 3140 | x |
| 18 | Air | 0.5 | 2.0 | 4050 | x |
| 19 | Air | 0.5 | 2.0 | 3450 | x |
| 20 | Air | 0.5 | 2.0 | 3770 | x |
| 21 | Air | 0.5 | 2.0 | 3860 | |
| 22 | Air | 0.5 | 1.9 | 3740 | |
| 23 | Air | 0.5 | 2.0 | 3810 | |
| 24 | Air | 0.3 | 1.9 | ≈3750 | |

## 3. Results

### 3.1. Post-flight analysis

Of the 24 tests, 18 aluminium spheres are recovered using the soft recovery system. Each sphere is then photographed, and the most interesting surface structures are photographed under a binocular magnifying glass.

The projectile can be eroded in the soft recovery system. In that case, the projectile surface appears as a blunt surface with granular structure. A previous study has shown that this erosion occurs when the impact velocity with the soft recovery is greater than $1500\,\mathrm{m \cdot s^{-1}}$ [4]. In the present experiment, the surface recession caused by the ablation cannot be accurately measured in post-flight because of this erosion. The surface recession caused by the ablation begins to be visible for initial speeds above $3300\,\mathrm{m \cdot s^{-1}}$ and are systematically visible for initial speeds above $3720\,\mathrm{m \cdot s^{-1}}$.

The occurrence of the ablation phenomenon during the flight is evidenced by the presence of a resolidified aluminium layer on the recovered projectiles. Smooth in appearance and forming an extra thickness on the sphere, this is the layer that melted during the model flight. This layer of molten aluminium is sheared off by the flow and convected towards the rear of the model. The presence of this resolidified layer indicates that the ablation stops during the flight because of the model deceleration. Pictures of this layer are shown in Fig. 3f and 3i and the pictures of the corresponding projectiles are shown in Fig.

3d, 3e, 3g and 3h. The stagnation region affected by the ablation extends up to an angle of $65$° to $90$°, depending on the test.

Six recovered models show roughness on the surface of the aluminium, as shown in Fig. 3a, 3b and 3c. These structures are composed of striated surfaces that are perpendicular to the flow. No significant parameter has yet been identified to explain the presence or absence of this roughness pattern. The appearance of roughness is a frequent phenomenon in ablation experiments, but there is no consensus on the cause [5]. In the case of striated surfaces, it seems that the combination of a homogeneous material with a turbulent boundary layer favours the development of this type of structure [6]. In the case of aluminium spheres, the striated surfaces are located on the sides of the sphere where the boundary layer is expected to become turbulent [7]. Duralumin becomes slightly pasty above $700$ K, and the striated surfaces could be a consequence that the surface temperature rising above this temperature without reaching the melting temperature.

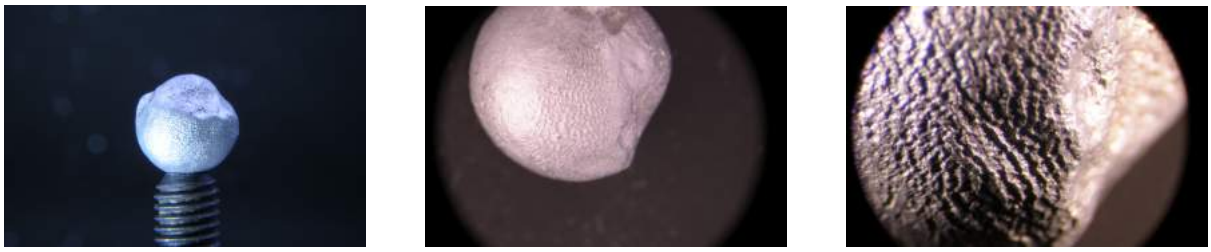

**(a)** Test n°16, low magnification **(b)** Test n°16, high magnification **(c)** Test n°16, detailed view

**(d)** Test n°17, low magnification **(e)** Test n°17, high magnification **(f)** Test n°17, detailed view

**(g)** Test n°18, low magnification **(h)** Test n°18, high magnification **(i)** Test n°18, detailed view

**Fig 3.** Pictures of recovered spheres

Finally the mass lost by the spheres is measured. The mass lost due to erosion within the soft recovery does not exceed $5$ % of the initial mass. The mass ratio $m/m_0$ for the spheres in case of ablation ranges from $96$ % up to $80$ %.

## 3.2. In-flight analysis

### *3.2.1. Velocity profiles*

The Fig. 4 presents the typical flight parameters calculated from the light barrier data for tests with muzzle velocities around $4000\,\mathrm{m}\cdot\mathrm{s}^{-1}$, an expansion tank pressure of $0.5$ bar and a measurement tunnel pressure of $2$ bar. The blue curve represents the part of the flight inside the expansion tank and the

orange curve the part inside the measurement tunnel. The interface between the two sections is represented by the position $0\,\mathrm{m}$. The green markers in Fig. 4a show the projectile positions detected by the light barriers.

The velocity is given by the Fig. 4b. The projectile flight is highly decelerated. The projectile impacts the soft recovery at a speed below $2000\,\mathrm{m\cdot s^{-1}}$ and can be recovered for post-flight analysis. The acceleration of the projectile is shown in Figure 4c and 4d. The maximum accelerations are reached at the entry of the measurement tunnel with $-1\cdot10^{6}\,\mathrm{m\cdot s^{-2}}$, i.e. $-275\,\mathrm{m\cdot s^{-1}\cdot m^{-1}}$, when the projectile speed is about $3770\,\mathrm{m\cdot s^{-1}}$.

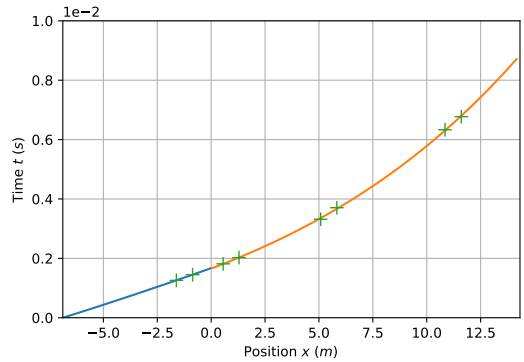


**(a)** Time in function of the flight distance

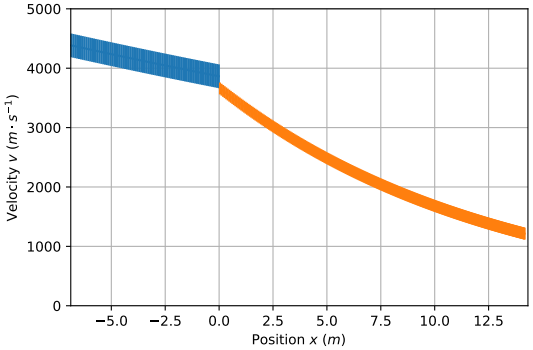


**(b)** Velocity in function of the flight distance

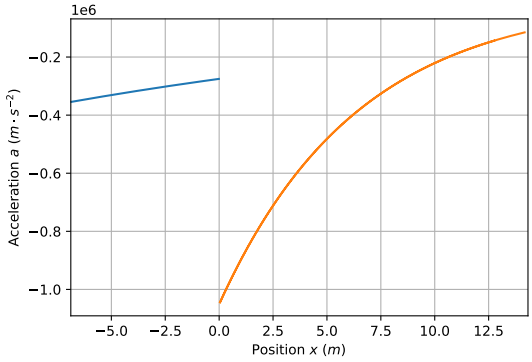


**(c)** Acceleration in function of the flight distance

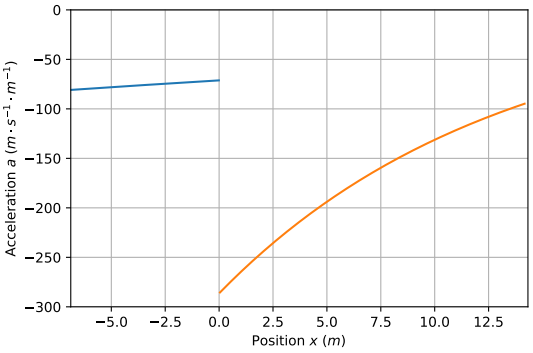


**(d)** Velocity decay in function of the flight distance

**Fig 4.** Velocity-Position-Time diagrams for the test n°20

By using the Eqn. 3, the drag coefficient of the sphere is evaluated from the velocity data. Since no ablation is detected in the tests n°5 and 6 and the velocity data are complete over the entire trajectory, these tests are used to calculate the drag coefficient of the non-ablated sphere. The drag coefficient of the sphere is estimated to be $0.89$ in agreement with the value of $0.9$ commonly found in the literature for a sphere in a hypersonic flow ([4], [8] & [9]). This demonstrates the ability to accurately measured the drag coefficient from the velocity data.

The study of the tests performed with pressure around $2\,\mathrm{bar}$ shows that the sphere is ablated along the trajectory. In case of ablation, the constant $Cx$ coefficient of the Eqn. 3 is superseded by an average deceleration coefficient $C_L$ given by Eqn. 4, which depends on the mass lost and the drag coefficient of the ablated sphere [4].

$$C_L = \frac{m_0}{m} Cx \tag{4}$$

The average deceleration coefficient for these tests is found to be $1.03$. If we assume a maximum variation of the drag coefficient of $\pm 10$ %, then the mass ratio $m/m_0$ is between $0.78$ % and $0.95$ %. These values correspond to the mass loss measured on the recovered spheres. By studying the deceleration coefficient $C_L$, we can determine whether ablation occurred during the flight. The measured coefficients are summarised in Tab. 3.

**Table 3.** Measured drag and deceleration coefficients

| $C_x$ *without ablation* | $C_L$ *with ablation* | $m/m_0$ *with ablation* |
|---|---|---|
| 0.89 | 1.03 | [0.78-0.95] |

### *3.2.2. Ablation in flight*

The Fig. 5 shows pictures of the spheres during the flight. Visualisations at the gun muzzle are shown on the left column. The projectile is visible in the centre of the pictures. The objects following the projectile are the sabots. The sphere emits a strong light as it leaves the launch tube. The thermal heating of the projectile during the acceleration phase is unknown. Future spectroscopic measurements at the muzzle are planned to detect the presence of aluminium in the wake of the projectile to assess whether the ablation could start inside the launch tube.

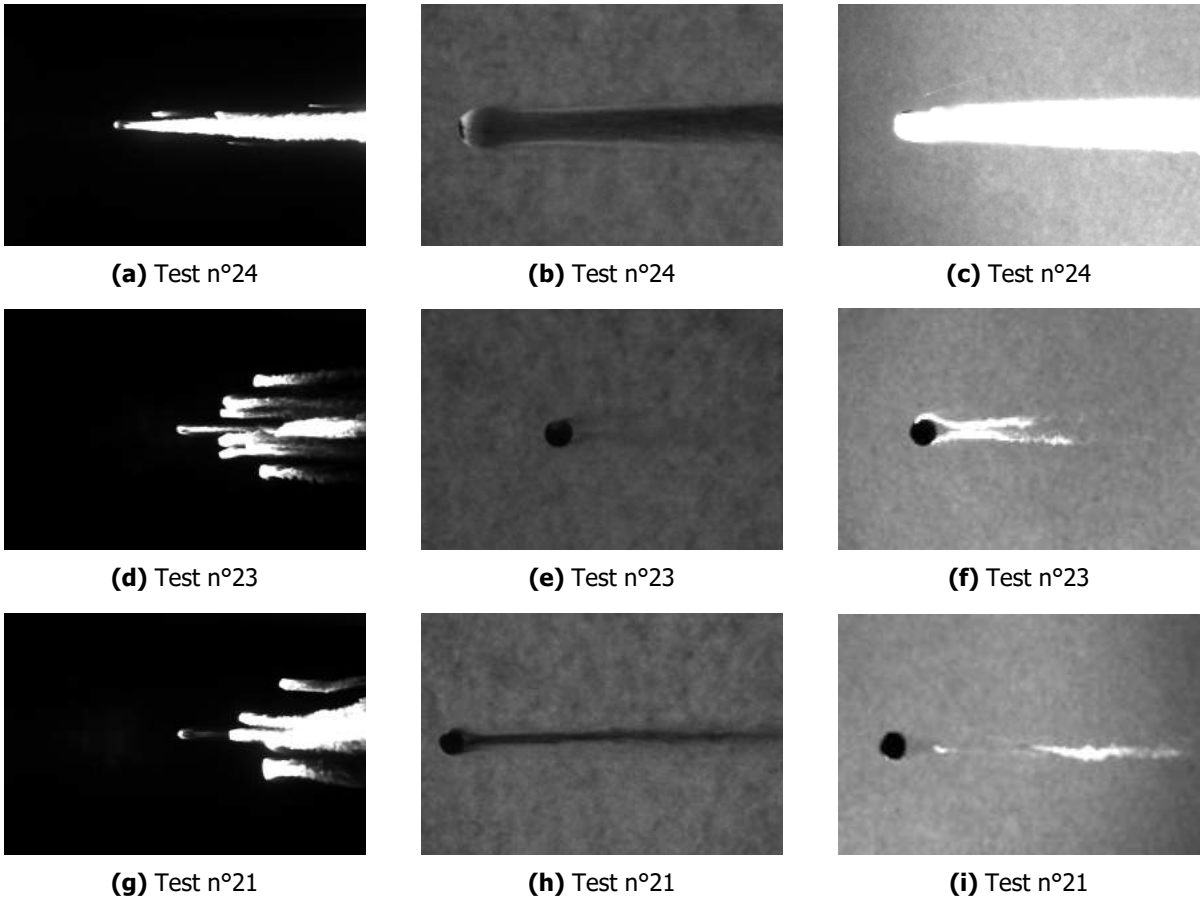

**(a)** Test n°24 **(b)** Test n°24 **(c)** Test n°24

**(d)** Test n°23 **(e)** Test n°23 **(f)** Test n°23

**(g)** Test n°21 **(h)** Test n°21 **(i)** Test n°21

**Fig 5.** Pictures of duralumin spheres in free flight in air. Left: view at the gun muzzle with a SAZ camera at $\Delta_{exp} = 160ns$. Center: view at $x = 2.0m$ with a SIMD16 camera at $\Delta_{exp} = 50ns$. Right: view at $x = 3.8m$ with a HPV-X camera at $\Delta_{exp} = 200ns$

The pictures shown in the middle and right columns clearly show the presence of ablation. In all tests carried out in air, where the ablation is confirmed, an ablation trail is visible in the wake, as in tests n°21, 23 and 24. There is also a strong light emission in the wake flow. This light emission is not visible in the tests performed in pure nitrogen. This indicates that the liquid aluminium is oxidised by the oxygen, producing light and releasing heat in the wake flow. For most of the tests in air, the light production is not directly observed at the stagnation point and is not axisymmetric. The position of the first light emission on the projectile surface cannot be precisely measured but is close to the position $30°$-$50°$ from the symmetry axis. At this location, the boundary layer is turbulent ([4] & [7]). The influence of the turbulence on the light emission should be investigated. It is assumed that turbulence allows a better diffusion of oxygen in the ablation layer and accelerates its oxidation.

In Fig. 6 the shadowgraphs confirm the previous observation. For the test n°23 performed in air, an intense light emission is visible at $1.3\,$m from the entry of the measurement tunnel, indicating that the ablation process begins quickly on the flight trajectory. For the test n°16, the surface roughness observed on the recovered sphere during the post-flight analysis is already visible on the shadowgraph. Indeed, multiple small shocks are observed on each side of the sphere at $90\,$deg from the symmetry axis.

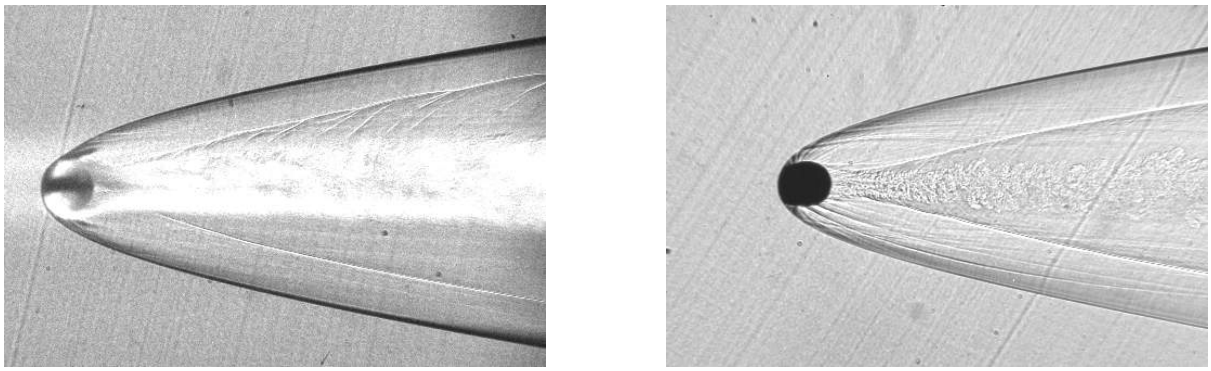

**(a)** Test n°23 (air) **(b)** Test n°16 (nitrogen)

**Fig 6.** Shadowgraphs at $x = 1.3m$ with a PCO camera at $\Delta_{exp} = 100ns$

Finally, for the tests where both the pictures and the flash radiographs are available, the surface recession of the duralumin spheres is computed at each measurement station. An image post-processing algorithm extracts the model contours for both types of images. It should be noted that the contour near the stagnation surface is only visible on the radiographs because the bow shock prevents optical visualisation of this zone. The Fig. 7 presents the model contours and the shock positions calculated at $1.3\,$m and $5.8\,$m from the tunnel entry. The black circle represents the initial 8mm-sphere. At $1.3\,$m no ablation is detected and the surface recession remains below the method uncertainty. However at $5.8\,$m a surface recession up to $0.2\,$mm is measured at the stagnation region. A third measurement station, located at the end of the free flight tunnel, measured the same model contour as the second station. For the cases with nitrogen, the ablation phenomenon starts soon after entering the measurement tunnel, but also stops in the first half of the tunnel. This is due to the model deceleration leading to a decrease in the wall heat flux. Similar results are obtained for the cases in air, where the ablation stops before the soft recovery system.

## 4. Conclusion

A method for the investigation of the ablation in hypersonic free flight is proposed. Experiments up to $4000\,\mathrm{m}\cdot\mathrm{s}^{-1}$ are performed. Compared to wind tunnel or plasma torch experiments the hyperballistic tunnel allows the study of dense and turbulent hypersonic flows. In addition, the inflow turbulence is quiet so that a natural laminar-turbulent transition is expected. However the light gas gun is limited to two experiments per day, which limits the total number of tests per measurement campaign.

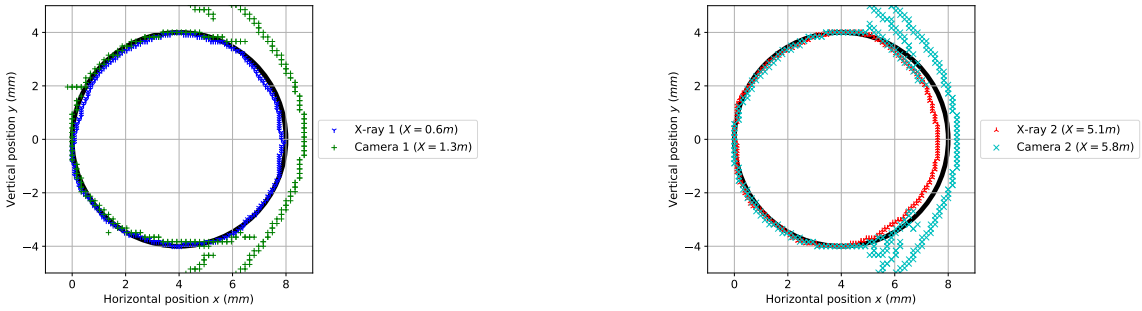


**(a)** $x_{tunnel} = 1.3m$ **(b)** $x_{tunnel} = 5.8m$

**Fig 7.** Model contours computed from the PCO images and the flash radiographs for the test n°10

The combination of the in-flight and post-flight analysis confirms the occurrence of the ablation phenomenon during the flight of the duralumin sphere. With the present test conditions, a minimum muzzle velocity of $3500\,\mathrm{m}\cdot\mathrm{s}^{-1}$ is required to heat the projectile to its melting point. If the temperature only approaches the melting point, a striated pattern is produced on the projectile surface. The flight data indicate that the ablation starts quickly after the tunnel entry but also stops when the projectile speed falls below about $2500\,\mathrm{m}\cdot\mathrm{s}^{-1}$. A new test campaign with several tests using the same conditions would confirm and refine these values.

From the velocity data, the analysis of the deceleration coefficients can predict the mass lost caused by the ablation, which is in agreement with the measured mass of the recovered spheres. Finally ablation profiles are measured during the flight by applying a contour detection algorithm to the optical and X-ray visualisations.

Based on this experimental methods, new measurement campaigns are planned to study the ablation of aluminium in free flight at quasi-constant speed and to study the ablation behaviour of other metallic materials.

## References

[1] R. Knikker, "Transferts thermiques," *Institut National des Sciences Appliquées de Lyon, Département Génie Mécanique Conception*, 2014-2015. (in French).

[2] H. Dubbel, K.-H. Grote, and J. Feldhusen, "Taschenbuch für den maschinenbau," *Springer*, 2007. https://doi.org/10.1007/978-3-540-68191-5. (in German).

[3] K. W. Naumann, "Die Erwärmung eines schweren KE-Geschoss über eine Flugbahn von $v_0 = 2500m/s$ bis $v_e = 2300m/s$," *French-Germain Research Institute of Saint-Louis*, 1994. (in German).

[4] J. Luneau, "Contribution à l'étude des phénomènes aérothermiques liés au vol hypersonique décéléré," *French-Germain Research Institute of Saint-Louis*, 1969. (PhD thesis, in French).

[5] H. W. Stock and J. J. Ginoux, "Hypersonic low temperature ablation an experimental study of cross-hatched surface patterns," *Astronautical Research 1971: Proceedings of the 22nd Congress of the International Astronautical Federation Brussels, 20–25 September 1971*, pp. 105–120, 1973.

[6] G. Duffa, "Ablative thermal protection systems modeling," *American Institute of Aeronautics and Astronautics, Inc.*, 2013. https://doi.org/10.2514/4.101717.

[7] F. Denis, "Study of the ablation by melting in hypersonic flow," *Strasbourg University*, 2022. (PhD thesis).

[8] A. J. Hodges, "The drag coefficient of very high velocity spheres," *Journal of the Aeronautical Sciences*, vol. 24, no. 10, pp. 755–758, 1957.

[9] J. D. Anderson Jr, "Hypersonic and high-temperature gas dynamics," *American Institute of Aeronautics and Astronautics*, 2006. https://doi.org/10.2514/4.861956.